

Bulk condensation by an active interface

Raushan Kant,^{1,*} Rahul Kumar Gupta,^{2,†} Harsh Soni,^{3,‡} A K Sood,^{1,§} and Sriram Ramaswamy^{1,¶}

¹*Department of Physics, Indian Institute of Science, Bangalore 560 012, India*

²*Sankhyasutra Labs Ltd., Manyata Embassy Business Park, Bengaluru, Karnataka 560 045, India*

³*School of Physical Sciences, Indian Institute of Technology Mandi, Kamand 175 005, India*

(Dated: April 4, 2024)

We present experiments, supported by mechanically detailed simulations, establishing bulk vapor-liquid condensation of a hard-bead fluid by a tiny population of orientable motile grains that self-assembles into a moving polarized monolayer. In a quasi-1D geometry two such layers, oppositely aligned, immobilize the condensed non-motile component. We account for our observations through a continuum theory with a naturally non-reciprocal Cahn-Hilliard structure, whose predicted trends as a function of packing fraction are consistent with our observations.

Subject areas: Physical Systems: Living matter & active matter

The persistent motility of active matter [1, 2] leads to a panoply of striking behaviours [3–7], of which condensation with neither attraction or depletion [8–13] and motile-nonmotile demixing [14–17] are the focus of the present work. In this article we report unexpected states of organisation in experiments, supported by mechanically detailed simulations, on mixtures of motile polar aligning rods and non-motile spherical beads. In dimensions $d = 1$ and 2, we find spontaneous segregation of polar rods and beads with increasing area fraction of either or both species.

The phenomenon persists down to exceptionally low rod fraction: a single row of motile polar rods is able to condense a bulk domain of beads, see Fig. 1. Thus a finite number, in $d = 1$, and a subextensive fraction in $d = 2$, of motile rods apparently affects an extensive population of beads. In $d = 2$, the rods self-assemble into a single row moving transverse to its length, forming a one-dimensional polarized active membrane, condensing the beads ahead of it [Fig. 2, movies SM1 & SM2 [18]]. In an annular channel with width much smaller than circumference, effectively $d = 1$ [Fig. 1, movies SM3 & SM4 [18]] the self-assembled structure is a robust, width-spanning, active piston. Upon increasing the rod fraction, two opposing pistons self-assemble to immobilize a macroscopic bead-dense domain, Fig. 3(a), movie SM5 [18]. The segregation can be understood physically through a positive-feedback argument: the moving rods force a bead-density gradient in the direction of their motion; their orientation is sterically adapted to point up this gradient. This mechanism operates through a coarse-grained theory for the dynamics of rod and bead densities, which naturally takes a non-reciprocal Cahn-Hilliard form [19–24]. Finally, we show theoretically that a localized motile rod density can transport a bead domain whose extent grows with its compression modulus, rationalizing the macroscopic condensation of beads. Our findings should have implications for spatial organization in living systems.

We now show how we obtained these results. Our ex-

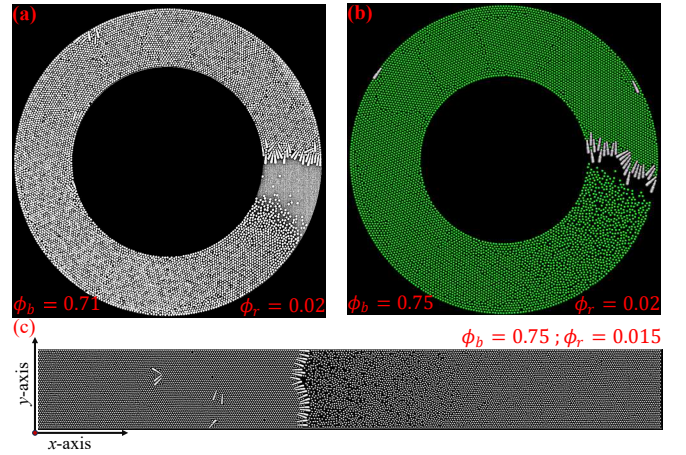


FIG. 1. A self-assembled monolayer of polar active particles condenses a bulk quantity of passive beads in (a) experiments and (b) mechanically detailed simulations on vibration-activated granular matter in an annular channel. The rod area fraction $\phi_r = 0.02$, bead area fraction $\phi_b = 0.71$ in experiment and $\phi_b = 0.75$ in simulation, if averaged over the entire domain. (c) The same phenomenon realized in simulations in a straight channel with dimensions 249×31 in units of the bead diameter, with periodic boundary conditions in the long dimension, at bead and rod area fractions $\phi_b = 0.75$ & $\phi_r = 0.015$.

perimental system consists of brass rods of length 4.5 mm, with thickness tapered from 1.1 mm to 0.7 mm from tail to nose, and spherical aluminium beads [25–30] of diameter 1 mm. The rod-bead mixture is confined between an anodised aluminium plate of diameter 12 cm and a glass lid, whose surfaces are separated by 1.12 mm. The plate is attached to a permanent magnetic shaker (LDS V406-PA100E). All experiments are done at a shaker frequency $f = 200$ Hz and amplitude $\mathcal{A} = 0.04$ mm, corresponding to a shaking strength $(2\pi f)^2 \mathcal{A} = 7$ times the acceleration due to gravity. We create an annular geometry by glueing a circular block at the centre of the sample cell; see Fig. 1(a). We capture im-

ages at six frames per second on a Redlake MotionPro X3 camera and post-process them on Fiji (ImageJ) for analysis in MATLAB and Python. We present complementary results from granular dynamics simulations as in [26, 29], with inter-particle and particle-wall interactions captured by an impulse-based collision model [31], including static friction and finite restitution. We use periodic boundary conditions (PBC) in the xy -plane to eliminate the complicating effect of lateral walls. In some cases we also re-create the experimental geometry [29] by way of confirmation. We set the static friction and restitution coefficients to 0.05 and 0.3 for particle-particle collisions, 0.03 and 0.1 for rod-base and rod-lid collisions, and 0.01 and 0.3 for bead-base and bead-lid collisions, respectively, in reasonable correspondence with the experimental system [26, 29, 32]. We have established the stationarity of our experimental nonequilibrium phases for at least 300 and, in several cases, 750 seconds. We use VMD software [33] to make simulation movies and snapshots.

For rod area fraction $\phi_r = 0$ the system displays fluid, hexatic and crystalline phases as a function of bead area fraction ϕ_b [30]. Prior studies of motile polar rods introduced into this system found flocking through a flow-induced interaction [26], and non-reciprocal pair interactions in crystalline [30] and dense fluid backgrounds [34]. Fig. 2(a) shows our experimental phase diagrams in the $\phi_b - \phi_r$ plane. For $d = 2$, at $\phi_b = 0.55$ and $\phi_r = 0.06$, the system is in the isotropic state, with particles distributed homogeneously and without organised motion or alignment. Across a first threshold $\phi_b = 0.70$, we see a transition to a homogeneous flock as in [26] with polar-rod orientations and all particle velocities aligned along the azimuthal direction. Past a second threshold $\phi_b = 0.75$, we observe rod-bead segregation. The third and most striking threshold ($\phi_b = 0.77$), marks the formation of a self-assembled row – a polar monolayer – of active rods, which condenses a bulk domain of beads [see Fig. 2(b) and movie SM6 [18]]. The rods align side by side, with their tapered tips pointing towards the dense, immobile region. The locus of the onset of this active self-assembly is $\phi_r + \phi_b \approx 0.83$. The bead domains on the two sides of the monolayer differ distinctly, though slightly, in packing fraction and considerably in mobility; see Fig. S1 [35] and movie SM1 [18]. Height fluctuations of the monolayer consistent with the existence of an interfacial tension are seen over a limited dynamic range, see Fig. S4 [35]. In simulations in a square domain with periodic boundary conditions, we find coherently moving self-assembled 1D membranes made of polar rods pointing from low to high density at $\phi_b = 0.80$ & $\phi_r = 0.03$ [see Fig. 2(c) and movie SM2 [18]]. Thus, our experiments and simulations allow an exceptionally small (and possibly sub-extensive) fraction of active rods to condense a bulk domain of passive beads.

Figs.1(a) and (b) show that the phenomenon persists

in experiments and simulations in the quasi-1D setting of an annular channel. For $\phi_b = 0.71$ and $\phi_r \simeq 0.02$, the system transitions from the isotropic phase to a state in which a self-assembled piston composed of just enough rods to fill a channel width separates bead-rich and bead-poor domains, see SM7 [18]. Rods initially dispersed throughout the medium in an isotropic state spontaneously undergo a high degree of spatial localization and azimuthal alignment. Fig. S2(b) shows that the bead medium is close-packed and nearly incompressible in front of the self-assembled active layer and exceedingly small behind it [35]. Fig. 1(c) from our simulations in a quasi-1D geometry with PBC along the x axis shows the formation of a self-assembled piston at large enough ϕ_b , reinforcing our experimental observation without the complication of a curved boundary. The self-assembled piston persists in simulation upon doubling the long dimension of the box with all other parameters unchanged; see SM8 [18]. We confirm the stationarity of the self-assembled state for over 2000 seconds; see SM3 [18]. In fact the sequence of phases – disordered to flock to condensation by active interface – with increasing ϕ_b at a given ϕ_r is seen in the quasi-1D system as well, [see Fig. 3(a) and movie SM9 [18]].

The most dramatic experimental demonstration of bulk condensation by an active boundary is seen in the quasi-1D geometry when the number of rods is sufficient to form two spanwise rows. In an ordered and segregated configuration, a subset of motile rods defects from the trailing to the leading edge of the moving bead domain, capturing and immobilizing it permanently on the time scale of our experiment, [see Figs. 3)(b), (c) and movie SM5 [18]]. Imposing a scalloped periphery [36] on the annular geometry facilitates the turning of the rods, augmenting this active capture, see Fig. 3, and leads to a stronger density enhancement in the condensed region, see Fig. S3 for characterisation of bead medium [35]. A self-sorting mechanism accounts for the stability of the balanced, immobile state: unequal rod populations at the two ends of a bead condensate will lead to net unidirectional motion, liberating rods at the trailing edge, which can turn and eventually be captured by the leading edge.

We note that active capture can be viewed as a 1D version of the core-halo state observed in motile/non-motile mixtures in [14]. In two dimensions, the steric interaction between our elongated motile particles promotes alignment, leading to extended domains with nearly straight boundaries rather than the irregular rafts of [14]. We now show that the mechanism and broad features of the demixing of active rods and passive beads can be understood within a coarse-grained theory. The hydrodynamic fields in our description are the number densities ρ and σ of beads and rods, obeying continuity equations $\partial_t \rho + \nabla \cdot \mathbf{J}_\rho = 0$, $\partial_t \sigma + \nabla \cdot \mathbf{J}_\sigma = 0$, with currents $\mathbf{J}_\rho = -D_\rho \nabla \rho - D_{\rho\sigma} \nabla \sigma + \alpha \rho \mathbf{P}$, $\mathbf{J}_\sigma = -D_\sigma \nabla \sigma - D_{\sigma\rho} \nabla \rho + u_0 \sigma \mathbf{P}$,

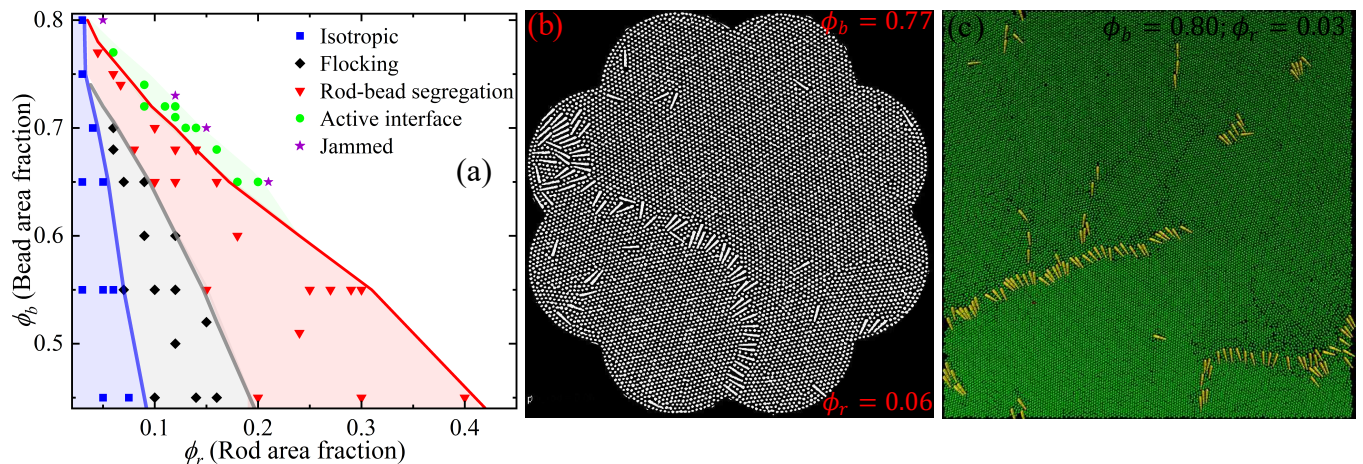


FIG. 2. (a) Experimental phase diagram in 2D in ϕ_b - ϕ_r plane, showing isotropic phase, flock, rod-bead segregation, and condensation by active interface, also see movie SM6 [18]. “Jammed” in the figure refers to a state in which extreme packing (total area fraction $\simeq 0.85$) leads to nearly arrested dynamics. (b) Bulk condensation of beads by an active interface of aligned rods in the experiment; $\phi_b = 0.77$ and $\phi_r = 0.06$. (c) Shows the travelling interface of aligned rods with PBC (along both directions) in square box simulation of length, 249 bead diameter; $\phi_b = 0.80$ and $\phi_r = 0.03$.

where the bare diagonal diffusivities D_ρ, D_σ and cross-diffusivities $D_{\rho\sigma}, D_{\sigma\rho}$ govern the *passive* dynamics (and hence $D_{\rho\sigma}D_{\sigma\rho} \geq 0$). Self-propulsion of rods with speed scale $u_0 > 0$, and active forcing of beads by rods with strength $\alpha > 0$ [26], are guided by the vector orientational order parameter field \mathbf{P} , which microscopically is the local average of unit vectors from the broad to the narrow end of the polar rods. We take $D_\rho, D_\sigma > 0$, as we are not in a regime where we expect either component to condense in the absence of interactions. \mathbf{P} in turn can be eliminated in favor of ρ, σ via a Landau theory modified by anchoring to density gradients with couplings A, B : $A\nabla\rho + B\nabla\sigma = (a + b|\mathbf{P}|^2)\mathbf{P}$, where we ignore flow-orientation couplings [26, 37] that merely shift parameter thresholds, and self-advection of \mathbf{P} [26, 38, 39] which affects our results at subleading order in gradients. Perturbing $\rho = \rho_0 + \delta\rho$, $\sigma = \sigma_0 + \delta\sigma$ deep in the disordered phase (a large and positive) yields the linear stability equations

$$\partial_t \delta\rho = \left(D_\rho - \frac{\rho_0 \alpha A}{a} \right) \nabla^2 \delta\rho + \left(D_{\rho\sigma} - \frac{\alpha \rho_0 B}{a} \right) \nabla^2 \delta\sigma, \quad (1)$$

$$\partial_t \delta\sigma = \left(D_{\sigma\rho} - u_0 \sigma_0 \frac{A}{a} \right) \nabla^2 \delta\rho + \left(D_\sigma - u_0 \sigma_0 \frac{B}{a} \right) \nabla^2 \delta\sigma. \quad (2)$$

whence we see the mechanism for bead condensation, in the form of a diffusively growing mode for large enough $\rho_0 \alpha A/a$, accessed, e.g., by increasing the bead concentration ρ_0 . We have implicitly assumed $\alpha A > 0$, for which we now argue, thus also recapitulating the feedback argument presented at the start of this article. Sterically, a rod’s narrow nose will fit more readily than its broad tail into a region of high bead density; so $A > 0$,

and rods power bead motion, creating ρ gradients in the direction of \mathbf{P} , hence $\alpha > 0$. Moreover, the independent activity parameters α and u_0 can cause beads to flee high rod density and rods to pursue high bead density, leading to opposite signs for the off-diagonal couplings in (1) in (2). This realizes the non-reciprocal Cahn-Hilliard system of [19, 20], with the added feature that even the phase separation is a consequence of activity. In the simplifying limit $D_\rho = 0$, $D_\sigma = 0$ & $D_{\sigma\rho} = 0$, the diffusive instability, that is bead condensation, arises for $A\alpha\rho_0 + Bu_0\sigma_0 > 0$, and non-reciprocity in the sense of off-diagonal couplings with opposite signs for $(A\alpha\rho_0 - Bu_0\sigma_0)^2 + 4AB\alpha\rho_0 u_0 \sigma_0 < 4aAD_{\rho\sigma}u_0\sigma_0$. These two conditions can coexist, e.g., for large enough $D_{\rho\sigma}$. More generally, decreasing $D_{\sigma\rho}$, say by increasing rod length, keeping other parameters fixed favors the emergence of non-reciprocity. When both instability and non-reciprocity are present, traveling spinodal patterns should arise as in [19, 20], a direction that remains to be explored in our experiments. Computational details and the equations for perturbations deep in the ordered phase ($-a = |a|$ large), where non-reciprocal effects enter at sub-leading order in wavenumber, are in the SI [35], with complete expressions for mode frequencies in Eq. (S10) and (S11).

Having established the mechanism for bulk rod-bead segregation, we finally return to the condensation of a *bulk* domain of beads by an *interfacial* population of motile rods. It suffices to examine the problem in one dimension. Details are in the Supplement [35]. For a closely related calculation see [34]. We replace the rods by a point force density $f\delta(x - v_0 t)$ moving with speed v_0 in the x direction, in a bead medium with density ρ

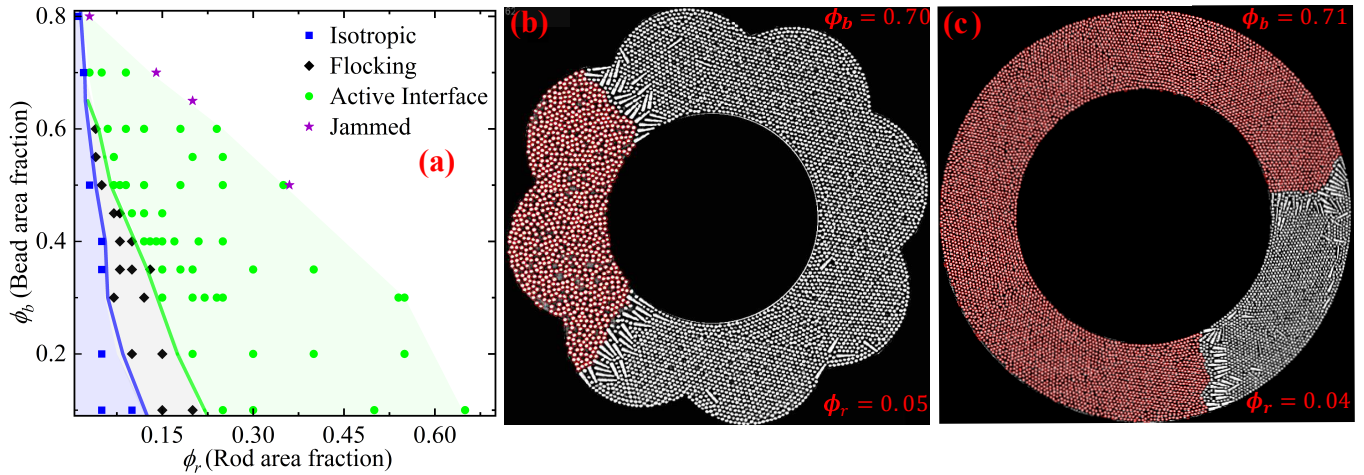


FIG. 3. (a) Phase-diagram in quasi-1D in ϕ_r - ϕ_b plane, which shows series of phases: isotropic, flocking to condensation by active interface, also see movie SM9 [18]. (b) and (c) shows a snapshot of condensation by two monolayers of rods in quasi-1D geometry with and without the floral outer boundary, with $\phi_b = 0.70$, $\phi_r = 0.05$ and $\phi_b = 0.71$, $\phi_r = 0.04$ respectively. The radius of the inner block in (b) and (c) is 2.5 and 4 cm respectively.

and current J_ρ , obeying force balance

$$\gamma J_\rho = -\partial_x \Pi(\rho(x)) + f\delta(x - v_0 t) \quad (3)$$

with a drag coefficient γ per bead and a general bead-pressure equation of state $\Pi = \Pi(\rho)$, and boundary conditions $\rho(x = -\infty) = \rho_0$, $\rho'(-\infty) = 0$. By suitable integration across the Dirac delta we show that

$$\Pi(\rho_+) - \Pi(\rho_-) = f \quad (4)$$

where ρ_+ , ρ_- are the densities on either side of the point force. If we approximate $\Pi'(\rho) \simeq \Pi'(\rho_0)$ for $x < 0$ and $\Pi'(\rho) \simeq \Pi'(\rho_+)$ for $x > 0$, we find $\rho(x < 0) \equiv \rho_0$ and

$$\rho(x > 0) = \rho_0 + (\rho_+ - \rho_0)e^{-x/\ell_+}, \quad \ell_+ \equiv \Pi'(\rho_+)/\gamma v_0, \quad (5)$$

with ρ_+ determined by $\Pi(\rho_+) - \Pi(\rho_0) = f$. A detailed solution must go beyond the approximation of a constant $\Pi'(\rho)$ and thus requires knowledge of the bead equation of state. For our purposes it suffices to know, from (5), that the extent of the bead domain, that is, the length scale ℓ_+ of the decay of the density with distance from the rod layer, is set by the stiffness $\Pi'(\rho_+)$. With increasing f , ρ_+ approaches maximum packing, so it becomes possible to push a bead domain of unlimited extent. Presumably, this is the mechanism at work in Fig. 1.

Before closing, we comment on other studies of active-passive segregation. In [16] small active particles condense domains of large passive particles through a depletion-like [40] mechanism. [10] examines the role of alignment of velocities and orientations, and [17] considers the effect of particle inertia. Our observations are related to the passive-core/active-halo segregation of [14, 15], but the domains in [14] are short-lived and limited in size, and the passive bands in [15] are of finite

width and are traversed by an active-particle flux. The absence of aligning interactions of the motile particles with each other or with density gradients is a key difference with respect to our work. An exception that just came to our notice is [41], in which the non-reciprocal interplay of alignment and density fields plays a central role.

We conclude with a summary of our results and a discussion of implications and open issues. Our experimental study of the nonequilibrium phase diagram of mixtures of shape-polar, motile or active rods with a steric tendency towards alignment and non-motile or passive spherical beads uncovers both bulk active-passive segregation and, more remarkably, bulk vapor-liquid condensation of the beads effected by the activity of an active interfacial layer or membrane of rods. A particularly striking effect in quasi-one-dimensional annular geometries is the formation of an immobile bulk domain of beads sequestered by two opposing active layers. We present a coarse-grained theory of this active condensation, based on the forcing of beads by motile rods and the steric tendency of rods to point in the direction of increasing bead density. The resulting diffusively growing mode presumably marks the limit of stability of the state of homogeneous bead density. The theory also predicts conditions under which the condensation should fail. Although the observed joint arrangement of rods and beads is precisely as implied by the above mechanism, our theory describes only the limit of linear stability, i.e., spinodal decomposition. Our observations, however, appear to be in a regime in which a self-assembled active layer of motile rods arises through nucleation. Further, we show analytically that the forcing generated by a localized active polar region can condense a macroscopic bead-rich do-

main ahead of it, whose density grows with the strength of the forcing and whose extent is limited only by its compressional stiffness, which in turn grows with the density. A theory taking into account the interplay with flocking and band formation as outlined in [42], and bridging the gap between monolayer and bulk concentrations of motile polar rods, is in progress. Finally, our discovery that a minuscule motile periphery suffices to sequester a macroscopic non-motile bulk introduces an original mechanism for condensation in living matter [43].

We have benefited from valuable discussions with M Barma, M E Cates, A Maitra, R Mondal, and M Rao. SR thanks the SERB, India for a J C Bose Fellowship, ICTS-TIFR for a Simons Visiting Professorship, the Isaac Newton Institute for Mathematical Sciences, Cambridge, for support and hospitality during the programme *Anti-diffusive dynamics: from sub-cellular to astrophysical scales* where work on this paper was undertaken, supported by EPSRC grant no EP/R014604/1, and ICTS-TIFR for support and hospitality during *Active Matter and Beyond*. RK was supported by the UGC, India, AKS acknowledges a National Science Chair Professorship of the DST, Government of India, and HS thanks the SERB, India, for support under grant no. SRG/2022/000061-G.

* raushankant@iisc.ac.in

† rahul.gupta09041@gmail.com

‡ harsh@iitmandi.ac.in

§ asood@iisc.ac.in

¶ sriram@iisc.ac.in

- [1] S. Ramaswamy, *Annual Review of Condensed Matter Physics* **1**, 323 (2010).
- [2] M. C. Marchetti, J. F. Joanny, S. Ramaswamy, T. B. Liverpool, J. Prost, M. Rao, and R. A. Simha, *Reviews of Modern Physics* **85**, 1143 (2013).
- [3] T. Vicsek and A. Zafeiris, *Physics Reports* **517**, 71 (2012), collective motion.
- [4] M. J. Bowick, N. Fakhri, M. C. Marchetti, and S. Ramaswamy, *Phys. Rev. X* **12**, 010501 (2022).
- [5] C. Bechinger, R. Di Leonardo, H. Löwen, C. Reichhardt, G. Volpe, and G. Volpe, *Rev. Mod. Phys.* **88**, 045006 (2016).
- [6] H. Chaté, *Annual Review of Condensed Matter Physics* **11**, 189 (2020).
- [7] G. Gompper, M. C. Marchetti, J. Tailleur, J. M. Yeomans, and C. Salomon, *Active Matter and Nonequilibrium Statistical Physics: Lecture Notes of the Les Houches Summer School* (Oxford University Press, 2022).
- [8] J. Tailleur and M. E. Cates, *Physical review letters* **100**, 218103 (2008).
- [9] Y. Fily and M. C. Marchetti, *Phys. Rev. Lett.* **108**, 235702 (2012).
- [10] S. R. McCandlish, A. Baskaran, and M. F. Hagan, *Soft Matter* **8**, 2527 (2012).
- [11] G. S. Redner, M. F. Hagan, and A. Baskaran, *Phys. Rev. Lett.* **110**, 055701 (2013).
- [12] M. E. Cates and J. Tailleur, *Annual Review of Condensed Matter Physics* **6**, 219 (2015).
- [13] D. Geyer, D. Martin, J. Tailleur, and D. Bartolo, *Physical Review X* **9**, 031043 (2019).
- [14] J. Stenhammar, R. Wittkowski, D. Marenduzzo, and M. E. Cates, *Phys. Rev. Lett.* **114**, 018301 (2015).
- [15] A. Wysocki, R. G. Winkler, and G. Gompper, *New journal of physics* **18**, 123030 (2016).
- [16] P. Dolai, A. Simha, and S. Mishra, *Soft Matter* **14**, 6137 (2018).
- [17] N. K. Agrawal and P. S. Mahapatra, *Phys. Rev. E* **104**, 044610 (2021).
- [18] “Supplementary movies,” (2023).
- [19] S. Saha, J. Agudo-Canalejo, and R. Golestanian, *Phys. Rev. X* **10**, 041009 (2020).
- [20] Z. You, A. Baskaran, and M. C. Marchetti, *Proceedings of the National Academy of Sciences* **117**, 19767 (2020).
- [21] S. Saha and R. Golestanian, *arXiv preprint arXiv:2208.14985* .
- [22] S. Saha, *arXiv preprint arXiv:2402.10057* (2024).
- [23] G. Tucci, R. Golestanian, and S. Saha, *arXiv preprint arXiv:2402.09279* (2024).
- [24] D. Greve, G. Lovato, T. Frohoff-Hülsmann, and U. Thiele, *arXiv preprint arXiv:2402.08634* (2024).
- [25] V. Narayan, *Phase Behaviour and Dynamics of an Agitated Monolayer of Granular Rods*, Ph.D. thesis (2010).
- [26] N. Kumar, H. Soni, S. Ramaswamy, and A. Sood, *Nature communications* **5**, 4688 (2014).
- [27] N. Kumar, R. K. Gupta, H. Soni, S. Ramaswamy, and A. K. Sood, *Phys. Rev. E* **99**, 032605 (2019).
- [28] P. K. Bera and A. K. Sood, *Phys. Rev. E* **101**, 052615 (2020).
- [29] H. Soni, N. Kumar, J. Nambisan, R. K. Gupta, A. K. Sood, and S. Ramaswamy, *Soft Matter* **16**, 7210 (2020).
- [30] R. K. Gupta, R. Kant, H. Soni, A. K. Sood, and S. Ramaswamy, *Phys. Rev. E* **105**, 064602 (2022).
- [31] W. J. Stronge, *Journal of Applied Mechanics* **61**, 605 (1994).
- [32] H. Soni, *Flocks, Flow and Fluctuations in Inanimate Matter: Simulations and Theory*, Ph.D. thesis (2019).
- [33] W. Humphrey, A. Dalke, and K. Schulten, *Journal of Molecular Graphics* **14**, 33 (1996).
- [34] J. P. Banerjee, R. Mandal, D. S. Banerjee, S. Thutupalli, and M. Rao, *Nature Communications* **13**, 4533 (2022).
- [35] R. Kant, R. K. Gupta, H. Soni, A. K. Sood, and S. Ramaswamy, “Supplementary information,” (2024).
- [36] J. Deseigne, O. Dauchot, and H. Chaté, *Phys. Rev. Lett.* **105**, 098001 (2010).
- [37] T. Brotto, J.-B. Caussin, E. Lauga, and D. Bartolo, *Phys. Rev. Lett.* **110**, 038101 (2013).
- [38] J. Toner and Y. Tu, *Phys. Rev. E* **58**, 4828 (1998).
- [39] J. Toner and Y. Tu, *Phys. Rev. Lett.* **75**, 4326 (1995).
- [40] S. Asakura and F. Oosawa, *The Journal of chemical physics* **22**, 1255 (1954).
- [41] K. L. Kreienkamp and S. H. L. Klapp, “Non-reciprocal alignment induces asymmetric clustering in active repulsive mixtures,” (2024), arXiv:2403.19291 [cond-mat.soft].
- [42] R. K. Gupta, *Simulations and Theory in Active Granular Matter: Nonequilibrium Phase Transitions and Non-reciprocal Interactions*, Ph.D. thesis (2021).
- [43] F. Jülicher and C. A. Weber, *Annual Review of Condensed Matter Physics* **15**, 237 (2024).

Bulk condensation by an active interface
Supplementary Material
(Dated: April 4, 2024)

arXiv:2403.18329v3 [cond-mat.soft] 3 Apr 2024

I. CHARACTERISTICS OF ROD-BEAD SEGREGATION

In this section, we characterise the nature of the bead medium and segregation of rods in the case of bead condensation by an interfacial minority of polar rods and active capture in the channel geometry. We characterise regions of bead medium that are free of rods. We use mean square displacement calculation to understand the mobility of the beads. For the interface state in two dimensions (floral geometry), the difference in the area fraction of region A (captured by interface) and region B (away from the interface) is not significant; for $\phi_b = 0.77$ & $\phi_r = 0.06$, it is 0.01 [see Fig. S1(a)]. However, the mobility difference remains substantial, as evident from the plots of mean-square displacement vs time [see Fig. S1(b)].

For the quasi-one-dimensional case, Fig. S2(b) illustrates the distribution of the bead medium about a self-assembled piston, highlighting the stark contrast in packing density on either side of the piston. In front of the piston, the bead medium is depicted as nearly close-packed, suggesting a near incompressibility due to the high density of beads. In the case of active capture, the difference in area fraction and the mobility of beads condensed by two monolayers of rods which we call dense (core) and rare (halo) regions, always remains significant; [see Fig. S3].

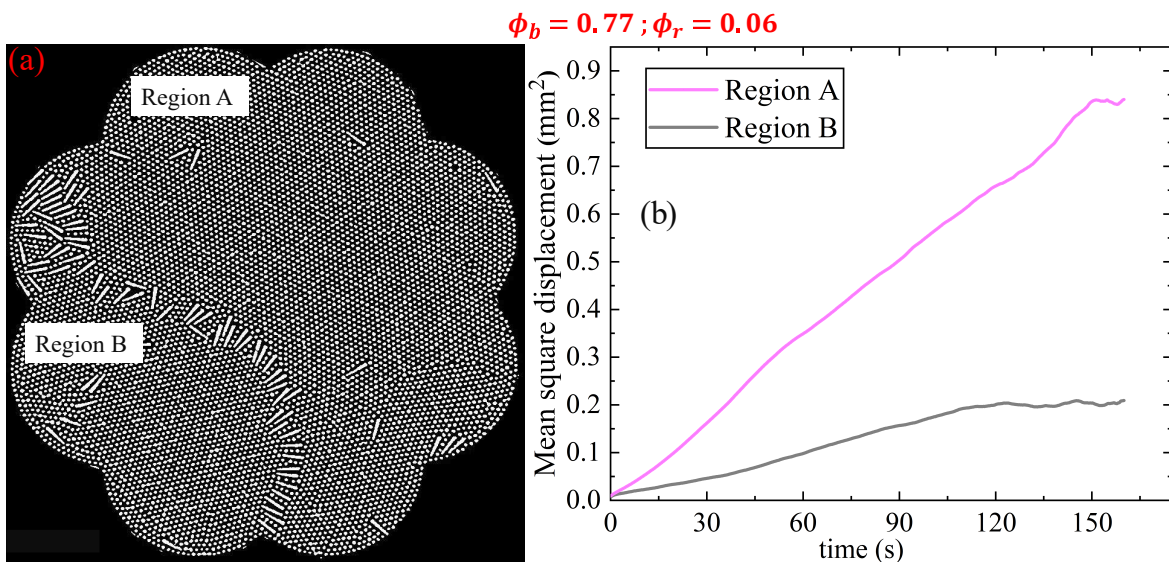


FIG. S1. Snapshot of interface state, $\phi_b = 0.77$ & $\phi_r = 0.06$: (a) A and B mark regions of low and high bead density respectively, segregated by an active polarized interface composed of rods pointing from A to B. (b) Mean-square displacement vs time for beads in the two regions, confirming that region B is less mobile than region A.

II. IDENTIFICATION OF THE INTERFACE

The forces driving our interface are distinct from those operating at thermal equilibrium and are akin to those arising in active membranes [1, 2]. However, over a modest range of length scales, we see behaviour corresponding to an emergent effective tension. Polar rods are sitting between two bead regions of different mobility so we choose them as the interface. However, a part of the interface constitutes more than one layer of rods. So, we analyse the part of the interface consisting of a monolayer of rods, see Fig. S4(a). We identify the interface by the line joining the centroids of the rods at the region dividing two bulk bead domains. There are a small number of rods sitting at the interface; we employ linear interpolation to define the height field $h(x, t)$ on scales smaller than the rod diameter, setting the resolution, $\Delta x = 1$ bead radius.

In Fig. S4(b) $\delta h(x, t)$ is plotted as the function of position x . We then calculate the Fourier component $\delta h_k(t) = \int_x \delta h(x, t) e^{-ikx}$ of $\delta h(x, t)$ using a discrete inverse Fourier transform and estimate the power spectrum $\langle |\delta h_k(t)|^2 \rangle$ to understand the scaling of interface fluctuations [3–5].

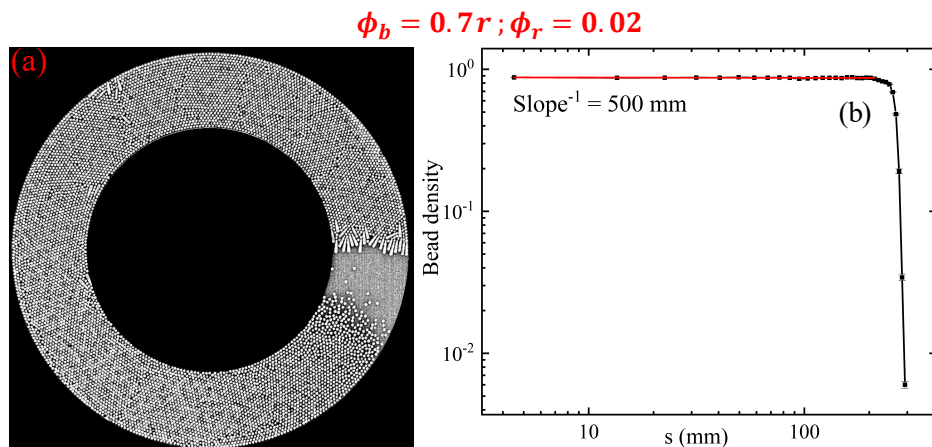


FIG. S2. (a) Snapshot of traveling condensed bead domain and active-rod monolayer. (b) Density profile of bead medium as a function of arc-length distance s from active monolayer, along the channel. The density profile of the bead medium in front of the piston decays very slowly and suddenly crashes. ϕ_b in front of the interface is ≈ 0.88 .

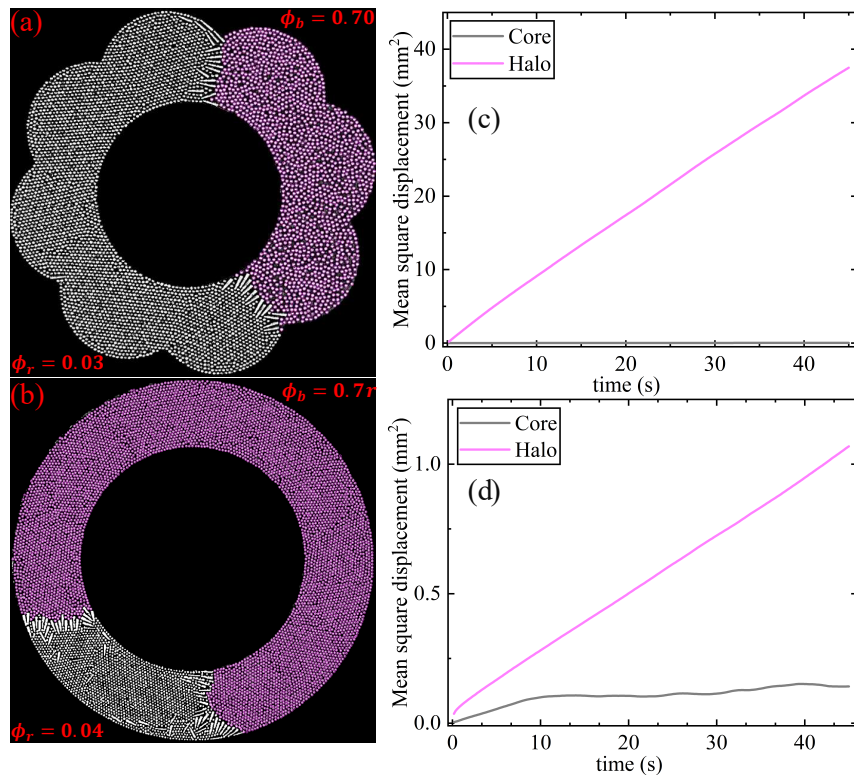


FIG. S3. Characterisation of the bead medium: (a) & (b) show the experimental snapshots of active capture observed in the quasi-one-dimensional case; the values of (ϕ_b and ϕ_r are mentioned in the figure). The bead area fraction values for the immobile crystalline core captured by the rods are $\phi_b = 0.84$ and $\phi_b = 0.85$ for (a) and (b), respectively. (c) & (d) show the stark difference between bead mean-square displacements in core and halo regions in the quasi-one-dimensional case.

III. COARSE-GRAINED THEORY AND STABILITY ANALYSIS

A. Dynamical equations

We draw on [6] to formulate the coupled dynamics of the polar orientational order parameter \mathbf{P} of the motile rods and the number densities ρ and σ of beads and rods. Note that \mathbf{P} should be viewed as the local average of the unit

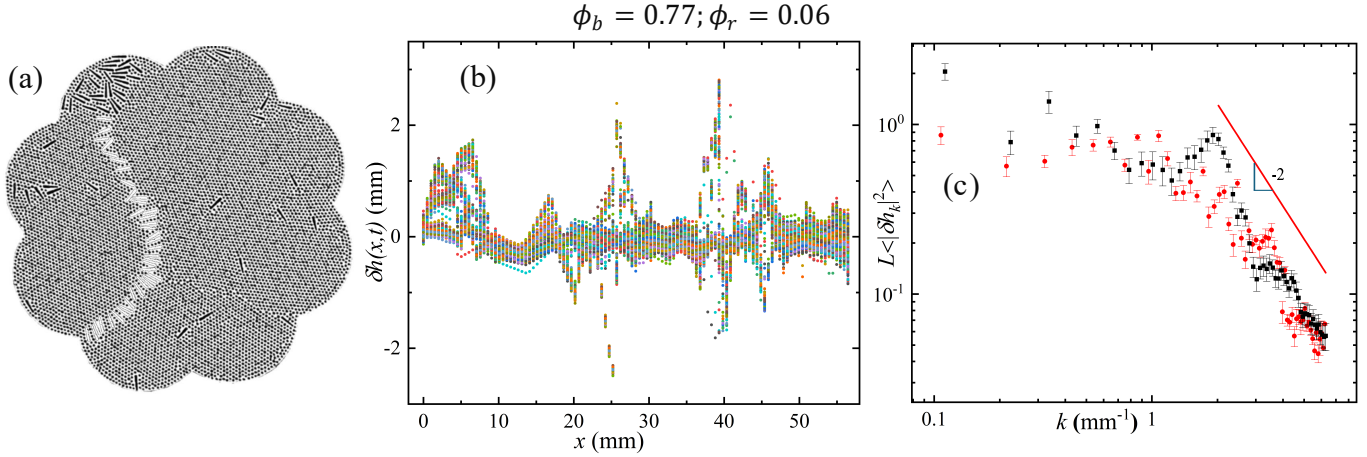


FIG. S4. Fluctuation spectrum of the active interface in two dimensions: (a) Snapshot of the active interface constituting rods stabilising a dense and immobile domain of beads at $\phi_b = 0.77$ & $\phi_r = 0.06$. We selected the masked line of rods to analyse the interface fluctuation. (b) Scatter plot of $\delta h(x, t) = h(x, t) - \langle h(x, t) \rangle_t$ vs x for all t , i.e., for all frames. Here $\langle h(x, t) \rangle_t$ is the time-averaged height profile. (c) Interface height fluctuation $L\langle |\delta h_k(t)|^2 \rangle$ vs wavenumber k averaged over more than 1000 frames at $\phi_b = 0.77$ and $\phi_r = 0.06$ in two different sets. Here L is the length of interface projected along the x -axis and k is the wavenumber; $L\langle |\delta h_k(t)|^2 \rangle$ scales as $1/k^2$ (line with slope -2 drawn to guide the eye) down to $k \simeq 1 \text{ mm}^{-1}$, that is, real-space scales of half a dozen rod diameters. We do not observe much dynamics on larger scales, possibly due to limited interface length, a curved mean profile, and the anchoring of the interface by the wall.

vectors of individual rods, defined to point from the broad to the narrow end or nose, which is also the direction in which they self-propel. We ignore the interplay [6, 7] of rod orientation with the hydrodynamic flow of beads, which if included only leads to finite shifts of thresholds. The conservation of beads and rods is expressed in the continuity equations

$$\partial_t \rho + \nabla \cdot \mathbf{J}_\rho = 0, \partial_t \sigma + \nabla \cdot \mathbf{J}_\sigma = 0 \quad (\text{S1})$$

with currents

$$\begin{aligned} \mathbf{J}_\rho &= -M_\rho \nabla \delta F / \delta \rho + \alpha \rho \mathbf{P} \\ &\simeq -D_\rho \nabla \rho - M_\rho w \nabla \sigma + \alpha \rho \mathbf{P} \end{aligned} \quad (\text{S2})$$

$$\begin{aligned} \mathbf{J}_\sigma &= -M_\sigma \nabla \delta F / \delta \sigma + u_0 \sigma \mathbf{P} \\ &\simeq -D_\sigma \nabla \sigma - M_\sigma w \nabla \rho + u_0 \sigma \mathbf{P}. \end{aligned} \quad (\text{S3})$$

Although our system is not thermal, we have assumed in (S2) and (S3) a reference equilibrium-like passive dynamics with diagonal mobility matrix $\text{diag}(M_\rho, M_\sigma)$. Cross-couplings between the two densities come from an interaction $w\rho\sigma$ in a free-energy functional F , leading to the direct and cross diffusive fluxes in (S2) and (S3). For hard particles the interaction is simply excluded volume, so $w > 0$. The collective diffusivities D_ρ, D_σ of rods and beads are determined by M_ρ, M_σ and thermodynamic parameters in F . This approach is reasonable, as the bead medium alone has a phase diagram resembling that of an equilibrium hard-sphere fluid [8]. We do not include noise in our coarse-grained treatment, though the diffusivities can be seen as originating in microscopic stochasticity. Active motion enters through u_0 and α which respectively set the scales of rod motility and forcing of bead motion by the rods, along the polarization \mathbf{P} [6]. We work directly with averaged quantities, but allow for spatial inhomogeneity. Extending Toner-Tu [9, 10] à la [6] gives

$$\partial_t \mathbf{P} = -(a + b\mathbf{P} \cdot \mathbf{P})\mathbf{P} + A\nabla \rho + B\nabla \sigma \quad (\text{S4})$$

with $b > 0$, and couplings A, B governing polar alignment with respect to density gradients. (S4) contains a (mean-field) transition to an ordered state with nonzero $\mathbf{P} = P\hat{\mathbf{x}}$ as a crosses from positive to negative, where $\hat{\mathbf{x}}$ is the spontaneously chosen direction of ordering. We work far from this flocking transition, either in the isotropic phase (a large and positive, with steady-state value $P = 0$) or deep in the ordered phase ($|a| = -a$ large and positive,

with $P = P_0 = \sqrt{|a|/b}$. The slow fluctuations of the order parameter transverse to $\hat{\mathbf{x}}$ in the symmetry-broken phase decouple from the densities in our linear theory and thus do not enter our treatment. We ignore self-advection of \mathbf{P} , which can be shown to enter the effective dynamics of the densities beyond diffusive order.

B. Linear stability analysis

On timescales $\gg 1/|a|$, the fast \mathbf{P} fluctuations are determined by those of the slow ρ and σ :

$$P = \frac{A}{a}\partial_x\rho + \frac{B}{a}\partial_x\sigma(\text{isotropic}); P = P_0 + \frac{A}{2|a|}\partial_x\rho + \frac{B}{2|a|}\partial_x\sigma(\text{ordered}), \quad (\text{S5})$$

where x is a generic direction in the isotropic phase and the direction of average polarization in the ordered phase. Perturbing $\rho = \rho_0 + \delta\rho, \sigma = \sigma_0 + \delta\sigma$ leads to the linear stability equations

$$\partial_t\delta\rho = \left(D_\rho - \frac{\rho_0\alpha A}{a}\right)\partial_x^2\delta\rho + \left(D_{\rho\sigma} - \frac{\alpha\rho_0 B}{a}\right)\partial_x^2\delta\sigma, \quad (\text{S6})$$

$$\partial_t\delta\sigma = \left(D_{\sigma\rho} - u_0\sigma_0\frac{A}{a}\right)\partial_x^2\delta\rho + \left(D_\sigma - u_0\sigma_0\frac{B}{a}\right)\partial_x^2\delta\sigma \quad (\text{S7})$$

in the isotropic phase and

$$\partial_t\delta\rho = -\alpha P_0\partial_x\delta\rho + \left(D_\rho - \frac{\rho_0\alpha A}{2|a|}\right)\partial_x^2\delta\rho + \left(D_{\rho\sigma} - \frac{\alpha\rho_0 B}{2|a|}\right)\partial_x^2\delta\sigma, \quad (\text{S8})$$

$$\partial_t\delta\sigma = -u_0 P_0\partial_x\delta\sigma + \left(D_{\sigma\rho} - u_0\sigma_0\frac{A}{2|a|}\right)\partial_x^2\delta\rho + \left(D_\sigma - u_0\sigma_0\frac{B}{2|a|}\right)\partial_x^2\delta\sigma \quad (\text{S9})$$

in the ordered phase, where $D_{\rho\sigma} \equiv M_\rho w$ and $D_{\sigma\rho} = M_\sigma w$. The stabilizing bare diffusivities $D_\rho, D_\sigma > 0$ compete with potential destabilization by the products of the active parameters α and u_0 , positive by definition, with the polar anchoring parameters A or B , whose sign defines the preferred heading of \mathbf{P} with respect to density gradients. While a microscopic calculation of these parameters is beyond the scope of this work, here is a plausible argument. A particle-dense region should accommodate the nose of a rod more readily than than its fat tail – rods like to point from low to high density – so the coefficients A and B in (S4) should be *positive*. Accepting this argument means all parameters appearing in Eqs. (S6) - (S9) are positive. For large enough $\rho_0\alpha A$, achieved for example by increasing the bead number density ρ_0 , vapor-liquid condensation of the beads should ensue. This is qualitatively consistent with the instability our experiments see. In addition, the term involving σ in (S6) or (S8) and that involving ρ in (S7) or (S9) can vary independently of each other, through the distinct activity parameters α and u_0 . It should then be possible to achieve opposite signs for $M_\rho w - \alpha\rho_0 B/a$ and $M_\sigma w - u_0\sigma_0 A/a$ in (S6) and (S7). For example, the rods, being large in size, should have lower mobility than the beads, $M_\sigma < M_\rho$. If so, with increasing activity, $M_\sigma w - u_0\sigma_0 A/a$ could well turn negative while $M_\rho w - \alpha\rho_0 B/a$ remained positive. Such an antagonistic off-diagonal coupling of ρ and σ is a realization of (the linearized part of) the non-reciprocal Cahn-Hilliard models of [11, 12]. The novelty of the present system is that not only the non-reciprocity but the phase-separation are a consequence of activity.

For disturbances of the form $\exp(iqx + st)$, (S6) - (S9) imply eigenvalues

$$s_\pm = \left[\frac{1}{2a} (A\alpha\rho_0 + Bu_0\sigma_0 - aD_\rho - aD_\sigma) \pm \frac{1}{2a} \sqrt{\{(A\alpha\rho_0 - Bu_0\sigma_0) - a(D_\rho - D_\sigma)\}^2 + 4(AB\alpha\rho_0 u_0\sigma_0 + a^2 D_{\rho\sigma} D_{\sigma\rho}) - 4a(BD_{\sigma\rho}\alpha\rho_0 + AD_{\rho\sigma}u_0\sigma_0)} \right] q^2 \quad (\text{S10})$$

for the isotropic phase and

$$s_{\pm} = \left[\frac{1}{4|a|} \{ (A\alpha\rho_0 + Bu_0\sigma_0) - 2|a|(D_{\rho} + D_{\sigma}) \} \right] q^2 - \frac{1}{2} iP_0(u_0 + \alpha)q \pm \sqrt{[4|a|^2(D_1^2 + 4D_{\rho\sigma}D_{\sigma\rho}) + (A_1 - B_1)^2 + 4B^2u_0\sigma_0\alpha\rho_0 - 4|a|(D_1(A_1 - B_1) + 2BD')]q^2 + i4P_0|a|u_1\{(A_1 - B_1) - 2|a|D_1\}q + 4P_0^2|a|^2u_1^2 \frac{q}{4|a|}}, \quad (\text{S11})$$

defining $D_1 = (D_{\rho} - D_{\sigma})$, $u_1 = (u_0 - \alpha)$, $(A_1 - B_1) = (A\alpha\rho_0 - Bu_0\sigma_0)$, $D' = D_{\rho\sigma}u_0\sigma_0 + D_{\sigma\rho}u_0\sigma_0$, for the ordered phase, that is, the flock.

IV. CONDENSATION OF A BULK DOMAIN OF BEADS BY AN ACTIVE INTERFACE

We return to the condensation of a *bulk* domain of beads by an *interfacial* population of motile rods. It suffices to examine the problem in one dimension. For a related treatment, see [13].

We replace the rods by a point force density $f\delta(x - v_0t)$ moving with speed v_0 in the x direction, in a bead medium with density and velocity fields ρ and v , obeying a continuity equation

$$\partial_t \rho + \partial_x(\rho v) = 0. \quad (\text{S12})$$

We ignore inertia and impose force balance

$$\gamma \rho v = -\partial_x \Pi(\rho(x)) + f\delta(x - v_0t) \quad (\text{S13})$$

on the beads, with a drag coefficient γ per bead and a general equation of state $\Pi = \Pi(\rho)$ for the pressure. Replacing v of (S12) from (S13) and comoving with a solution rigidly translating with velocity v_0 gives Eqs. (S12) and (S13), for a rigidly comoving solution with velocity v_0 yield

$$\partial_x \rho + \frac{1}{\gamma v_0} \partial_x^2 \Pi = \frac{f}{\gamma v_0} \delta'(x), \quad (\text{S14})$$

which gives the density jump

$$\rho_+ - \rho_- = (1/\gamma v_0) (\partial_x \Pi_- - \partial_x \Pi_+). \quad (\text{S15})$$

Integrating (S14) from $-\infty$ to x , with $\rho(-\infty) = \rho_0$, $\rho'(-\infty) = 0$ gives

$$\rho(x) - \rho_0 + \frac{1}{\gamma v_0} \partial_x \Pi(\rho(x)) = \frac{f}{\gamma v_0} \delta(x) \quad (\text{S16})$$

which, upon integration across the Dirac delta, yields the pressure jump

$$\Pi(\rho_+) - \Pi(\rho_-) = f \quad (\text{S17})$$

created by the forcing f of the rods. For $x < 0$: (S16) \implies

$$\frac{\Pi'(\rho)d\rho}{\rho - \rho_0} = -\gamma v_0 dx \quad (\text{S18})$$

which, if we approximate $\Pi'(\rho) \simeq \Pi'(\rho_0)$, gives

$$\rho(x) = \rho_0 + Ae^{-x/\ell_-}, \text{ with } \ell_- = \frac{\Pi'(\rho_0)}{\gamma v_0}, \quad (\text{S19})$$

forcing $A = 0$ to satisfy $\rho(-\infty) = \rho_0$, so that $\rho(x < 0) \equiv \rho_0$. For $x > 0$ we integrate (S14) from $0+$ to x and use $\partial_x \Pi(x) = \Pi'(\rho)\rho'(x)$ to get

$$\rho(x) - \rho_+ + \frac{1}{\gamma v_0} [\Pi'(\rho(x))\rho'(x) - \Pi'(\rho_+)\rho'_+] = 0 \quad (\text{S20})$$

which, from (S15) and $\rho_- = \rho_0$, implies

$$-\Pi'(\rho)\rho'(x) = \gamma v_0(\rho - \rho_0) \quad (\text{S21})$$

Approximating $\Pi'(\rho) \simeq \Pi'(\rho_+)$ for $x > 0$ then yields the solution

$$\rho(x > 0) = \rho_0 + (\rho_+ - \rho_0)e^{-x/\ell_+}, \ell_+ \equiv \Pi'(\rho_+)/\gamma v_0 \quad (\text{S22})$$

and, from (S17), ρ_+ is determined by $\Pi(\rho_+) - \Pi(\rho_0) = f$. A detailed solution must go beyond the approximation of a constant $\Pi'(\rho)$ and thus requires knowledge of the bead equation of state.

V. DESCRIPTION OF SUPPLEMENTARY MOVIES

File name: SM1Interface

Description: Fluctuating interface constituting polar rods at $\phi_b = 0.77$ and $\phi_r = 0.06$, in two-dimensional case.

File name: SM2PBCXY

Description: Travelling self-assembled 1D membranes made of polar rods pointing from low to high density at $\phi_b = 0.80$ & $\phi_r = 0.03$ in square box simulations with periodic boundary conditions with dimensions of 249 bead diameter

File name: SM3PBCX

Description: Video of moving piston assembly in simulation with dimensions 249×31 in units of the bead diameter, with periodic boundary conditions; $\phi_b = 0.75$ & $\phi_r = 0.015$.

File name: SM4ExpAnnular

Description: Video of moving piston assembly in the experiment in quasi-one-dimensional case; $\phi_b = 0.71$ & $\phi_r = 0.02$.

File name: SM5ActiveCaptureExp

Description: Condensation of beads by the two mono-layer of motile polar rods in the quasi-one-dimensional case at $\phi_b = 0.70$ and $\phi_r = 0.05$ with the time stamp.

File name: SM6Transition2D

Description: Phase transition with increasing ϕ_b at $\phi_r = 0.06$, in the two-dimensional case: isotropic phase, $\phi_b = 0.55$, flocking, $\phi_b = 0.70$, rod-bead segregation at $\phi_b = 0.75$ and active interface $\phi_b = 0.77$.

File name: SM7TransitionAnnularQuasi1D

Description: Phase transition with increasing ϕ_r at $\phi_b = 0.71$, in quasi-one-dimensional case showing isotropic phase, $\phi_r = 0.01$, travelling Active Interface, $\phi_r = 0.02$ and capture at $\phi_r = 0.04$.

File name: SM8

Description: Video of travelling active interface showing this phenomenon persists in simulation upon doubling the box length in the long dimension; $\phi_b = 0.75$ & $\phi_r = 0.02$

File name: SM9TransitionChannelGeometryQuasi1D

Description: Phase transition with increasing ϕ_b at $\phi_r = 0.05$, in quasi-one-dimensional case with outer floral boundary showing isotropic phase, $\phi_b = 0.20$, flocking, $\phi_b = 0.50$ and capture at $\phi_b = 0.70$.

File name: SM10Simulationquasi1D

Description: Video of moving piston assembly in the simulation in annular geometry; $\phi_b = 0.75$ & $\phi_r = 0.02$.

-
- [1] S. Ramaswamy, J. Toner, and J. Prost, *Phys. Rev. Lett.* **84**, 3494 (2000).
 - [2] H. Turlier and T. Betz, *Annual Review of Condensed Matter Physics* **10**, 213 (2019).
 - [3] C. del Junco and S. Vaikuntanathan, *The Journal of Chemical Physics* **150**, 094708 (2019).
 - [4] A. Patch, D. M. Sussman, D. Yllanes, and M. C. Marchetti, *Soft Matter* **14**, 7435 (2018).
 - [5] S. Gokhale, K. H. Nagamanasa, R. Ganapathy, and A. K. Sood, *Soft Matter* **9**, 6634 (2013).
 - [6] N. Kumar, H. Soni, S. Ramaswamy, and A. Sood, *Nature communications* **5**, 4688 (2014).
 - [7] T. Brotto, J.-B. Caussin, E. Lauga, and D. Bartolo, *Phys. Rev. Lett.* **110**, 038101 (2013).
 - [8] J. Olafsen and J. Urbach, *Physical review letters* **95**, 098002 (2005).
 - [9] J. Toner and Y. Tu, *Phys. Rev. Lett.* **75**, 4326 (1995).
 - [10] J. Toner and Y. Tu, *Phys. Rev. E* **58**, 4828 (1998).
 - [11] S. Saha, J. Agudo-Canalejo, and R. Golestanian, *Phys. Rev. X* **10**, 041009 (2020).
 - [12] Z. You, A. Baskaran, and M. C. Marchetti, *Proceedings of the National Academy of Sciences* **117**, 19767 (2020).
 - [13] J. P. Banerjee, R. Mandal, D. S. Banerjee, S. Thutupalli, and M. Rao, *Nature Communications* **13**, 4533 (2022).